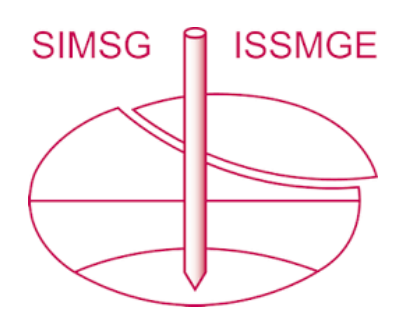
INTERNATIONAL SOCIETY FOR SOIL MECHANICS AND GEOTECHNICAL ENGINEERING



This paper was downloaded from the Online Library of the International Society for Soil Mechanics and Geotechnical Engineering (ISSMGE). The library is available here:

https://www.issmge.org/publications/online-library

This is an open-access database that archives thousands of papers published under the Auspices of the ISSMGE and maintained by the Innovation and Development Committee of ISSMGE.

The paper was published in the Proceedings of the 8th International Symposium on Deformation Characteristics of Geomaterials (IS-PORTO 2023) and was edited by António Viana da Fonseca and Cristiana Ferreira. The symposium was held from the 3rd to the 6th of September 2023 in Porto, Portugal.



Influence of the coefficient of uniformity on bio-cemented sands: a microscale investigation

Marlee Reed^{1#} and Brina M. Montoya¹

¹North Carolina State University, Department of Civil, Construction, and Environmental Engineering, 915 Partners Way Raleigh, NC 27607, USA **Corresponding author: mdstrong@ncsu.edu

ABSTRACT

Microbially induced carbonate precipitation (MICP) is a bio-mediated ground improvement technique that can increase soil stiffness and produce cohesion within granular material. Most experimental investigations on MICP-treated soils are performed on idealized granular materials. Evaluating a narrow range of particle sizes dismisses the potential influence of soil fabric on MICP treatment efficiency. Therefore, little is known regarding the influence of soil fabric on the level of improvement achievable post-MICP treatment. We investigate the influence of the coefficient of uniformity (C_u) on the level of improvement that can be obtained from MICP treatment. This study couples unconfined compression testing with microscale observations obtained from x-ray computed tomography (CT) of two sand mixtures with different C_u values. A soil column and CT specimen of each sand mixture were prepared and received the same number of MICP-injections. The shear wave velocity (V_s) of the soil columns was monitored to evaluate the increase in soil stiffness over time. After MICP treatment, the bio-cemented columns were subjected to unconfined compressive strength testing. Results indicate that for a similar mass of carbonate, the soil with a larger C_u experienced a greater increase in V_s but a lower maximum unconfined compressive strength. Through CT imaging, the soil with a smaller C_u was observed to have a more uniform distribution of carbonate within the sand matrix whereas the soil with a larger C_u has more sporadic MICP trends. This study elucidates the influence of soil fabric on the level of improvement that can be achieved through MICP treatment and assesses the reliability of x-ray CT scanning of MICP-treated sands with moderate carbonate content.

Keywords: Microbially induced calcium carbonate precipitation; x-ray computed tomography; unconfined compressive strength; coefficient of uniformity.

1. Introduction

Microbially induced carbonate precipitation (MICP) has seen increasing research interest over the past two decades (DeJong et al. 2010, DeJong et al. 2022). MICP uses bacteria as a catalyst for urea hydrolysis, creating favorable conditions within a soil matrix for carbonate precipitation. Current knowledge indicates preferential precipitation deposits at particle-particle contacts (DeJong et al. 2010). Particle-particle MICP bonding enables an increase in soil stiffness that can be observed from shear wave velocity (V_s) measurements (Montoya et al. 2012, Montoya and DeJong 2015) and unconfined compressive strength (UCS) testing (Al Qabany and Soga 2013). The improvement in stiffness along with transition from contractive to dilative volumetric response (Montoya and DeJong 2015) makes MICPtreated soils a viable soil improvement technique for liquefaction mitigation (DeJong et al. 2022).

In the early development of MICP as a soil improvement technique, a majority of the test materials used for MICP research were Ottawa sands (DeJong et al. 2010, Montoya and DeJong 2015, DeJong et al. 2022). Ottawa sands have quartz mineralogy, high roundness, high sphericity, and a narrow range of particle sizes. Additionally, Ottawa sand is a widely available standardized test material, making it favorable for

international research collaboration and establishing MICP protocol (DeJong et al. 2022). However, limited subsurface soils can be represented by Ottawa sands. Therefore, using Ottawa sands to assess the level of improvement from MICP has become limited. The idealizations, as a result of studying spherical grains with a narrow range of particle sizes, prohibits a meaningful evaluation of the intrinsic sand characteristics on MICP efficiency.

Numerous researchers have acknowledged the limitations associated with using Ottawa sands and have started to evaluate the MICP efficiency of test materials with different intrinsic characteristics (Lin et al. 2016, Nafisi et al. 2020, DeJong et al. 2022). Such characteristics may include mean particle size (D₅₀), coefficient of uniformity (Cu), and particle morphological parameters such as sphericity, roundness, or aspect ratio. Most studies have focused on evaluating differences in macroscale behaviour, such as soil strength, as a result of varying soil characteristics. Lin et al. (2016) and Nafisi et al. (2020) observed that mean particle size (D₅₀) influences the shear response of MICPtreated sand in triaxial compression. Lin et al. (2016) found that Ottawa 20/30 sand experienced a greater increase in peak shear strength than Ottawa 50/70 sand for similar calcium carbonate contents. In addition to studying particle size, Nafisi et al. (2020) found that the same improvement in V_s required a larger calcium

carbonate content for subangular sand grains compared to rounded sand grains. Both of these studies (Lin et al. 2016, Nafisi et al. 2020) coupled their experimental testing programs with scanning electron microscopy (SEM) to observe changes in soil microstructure that influenced the macroscale response.

It has become state-of-practice for MICP researchers to include SEM images in their experimental testing program. These two-dimensional viewing planes allow researchers to identify the carbonate polymorphs (e.g. calcite, aragonite, vaterite) present and qualitatively assess the relative size of MICP deposits. However, two-dimensional images cannot evaluate three-dimensional soil microstructure, particularly for non-uniformly graded soils. X-ray computed tomography (CT) is a non-destructive imaging technique that overcomes the two-dimensional limitations of SEM images and captures a three-dimensional soil system.

X-ray CT is a relatively new approach used to study particulate media. Several researchers have explored the potential of using x-ray CT to study MICP-treated sands (Tagliaferri et al. 2011, Dadda et al. 2017, Baek et al. 2022). Tagliaferri et al. (2011) performed x-ray CT on a bio-cemented triaxial specimen at different stages during loading to study shear band formation. Dadda et al. (2017) used CT scanning to study the changes in porosity, specific surface area, and permeability of MICP-treated sand. Both of these studies used a test material with D_{50} of 0.2 mm and C_u of 1.5. Back et al. (2022) studied the porosity reduction over time for two MICP-treated sands with D_{50} of 1.3 and 3.0 mm and calcium carbonate contents greater than 20%. These studies used x-ray CT to gain insight to changes in soil fabric during MICP treatment. However, previous studies have not evaluated the influence of varying C_u on MICP efficiency.

To better understand how sand fabric affects the level of improvement that can be achieved from MICP treatment, the current study evaluates the soil stiffness, strength, and microstructure of two MICP-treated sand mixtures with varying C_u . The evolution of soil stiffness is studied by monitoring the V_s of the soil columns during MICP treatment. After receiving the targeted number of MICP-injections, the bio-cemented columns are subjected to UCS testing to quantify differences in strength as a result of MICP at particle-particle contacts. Finally, x-ray CT is used to observe variations in soil microstructure due to the influence of C_u and calcium carbonate content.

2. Materials and Methods

2.1. Sample preparation

Two sands from the same quarry source with different C_u values but similar D_{50} values were evaluated in this study (Table 1). Both silica sand mixtures have subangular to subrounded particle morphology. Additional sand properties are provided in Table 1.

Four soil columns were prepared to a relative density of approximately 40% using dry pluviation techniques. Each specimen had a height and diameter of approximately 50 mm.

The specimens were kept under a low confining pressure (30 kPa) during MICP treatment.

A thin-walled 5 mL syringe was selected for CT specimen preparation for its size compatibility with the CT scanning equipment. The inside diameter of the syringe (12.4 mm) is approximately six times greater than the maximum particle size of the sand mixture with a C_u of 3.8. Glass wool was used as a filter at the bottom of the syringe and as a restraint at the top of the sand specimen (Fig. 1b). The specimen were prepared using air pluviation techniques; however, the initial void ratio could not be experimentally determined due to the glass wool layers. Additionally, the confining pressure applied to the sand grains by the top layer of glass wool could not be determined.

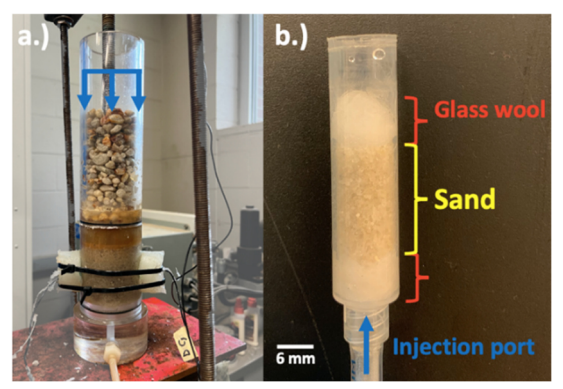


Figure 1. Sample preparation of a.) column specimen with bender elements for UCS testing and b.) CT specimen for imaging.

2.2. Microbially induced cementation

The bacteria *Sporosarcina pasteurii* (ATCC 11589) was used as the catalyst for urea hydrolysis to induce calcium carbonate precipitation within the soil matrix. The bacterial growth medium was prepared using 20 g/L yeast extract, 10 g/L ammonium sulfate, and 0.13 mol/L Tris buffer. The bacterial solution was incubated at 30°C at 200 rpm for approximately 24 hours to obtain an OD_{600} between 0.8 and 1.2. The solution was then centrifuged at 4000 rpm for 15 minutes. The centrifuged bacteria were stored for up to 14 days at 4°C.

Both the soil column and CT specimens were flushed with 10 pore volumes of deaired water before starting MICP treatment to achieve saturated conditions. Surface percolation was used to initiate flow within the soil column specimen. The head was kept above the height of the specimen to ensure the specimen would not become unsaturated. The CT specimen were flushed from bottom to top using a syringe.

The column and CT specimen were MICP-treated concurrently. The biological treatment solution contained 333 mM urea, 374 mM ammonium chloride, and 15 mL suspended bacteria per 100 mL of biological solution. After the biological treatment solution was administered, a 12 hour retention time was allowed to provide sufficient time for bacterial attachment within the soil matrix. Following the retention time, approximately 2 pore volumes of cementation solution was administered followed by a 6 or 12 hour waiting time between injections.

Table 1. Characteristics of test materials

	D ₅₀ (mm)	D ₁₀ (mm)	Cu	Ce	G_s	emin	emax
Cu1.3	0.72	0.56	1.3	0.99	2.65	0.53	0.79
Cu3.8	0.70	0.25	3.8	0.79	2.65	0.37	0.63

The cementation solution contained 333 mM urea, 374 mM ammonium chloride, and 100 mM calcium chloride. The specimen received a total of 18 cementation injections (e.g., Cu1.3_18i, Cu3.8_18i) or 30 cementation injections (e.g., Cu1.3_30i, Cu3.8_30i). Additional suspended bacteria was added to the cementation solution on every fourth injection.

2.3. MICP process monitoring

The V_s of the columns was monitored every 6 hours during MICP treatment using bender elements. An increase in V_s indicates cementation has developed at particle-particle contacts. Bender elements were prepared following the protocol established in Montoya et al. (2012). The bender elements were embedded mid-height on the acrylic column mold. A 10V sinusoidal wave was generated using a signal generator and the sending wave was received by an oscilloscope. The transmitting sinusoidal wave was sent at frequencies ranging from 1 – 20 kHz using a frequency sweep to determine the clearest received signal; the resonance frequency of the bender elements was expected to change as the stiffness of the soil changed (Montoya et al. 2012). The travel time and distance between the transmitting and receiving bender elements were used to calculate the V_s.

2.4. Unconfined compressive strength testing

Following MICP treatment, the column specimen were extruded from the acrylic, cylindrical mold using a Shelby tube extruder. UCS tests (ASTM D2166) were performed at a strain rate of 1%/min. The height and diameter of the specimen were measured before UCS testing and the appropriate height to diameter correction factor was used to process the data.

2.5. Calcium carbonate determination

After shearing the UCS specimen to failure, the top and bottom portions of the specimen were collected to determine the mass of calcium carbonate, following the gasometric method outlined in O'Toole et al. (2022). The CT specimen were extruded from the sample preparation syringe after imaging to determine the calcium carbonate content. A range of mass of pure calcium carbonate was dissolved by 1M hydrochloric acid and the resulting volumes of carbon dioxide gas from dissolution were used to develop a calibration curve. The calibration curve was used to interpret the calcium carbonate content of the soil. The calcium carbonate content of the untreated soil was also determined and subtracted from the MICP-treated sand carbonate content, as recommended in DeJong et al. (2022).

2.6. CT scan properties

The sand specimen were imaged using a Xradia 510 Versa 3D X-ray microscope (Zeiss, Germany) at 160 kV using the 4X objective lens. The same source-to-specimen and specimen-to-detector distances were used for each scan. 1601 projections were taken, resulting in high resolution images with a pixel size of 1.18 µm. The software XMReconstructor was used to reconstruct 8-bit TIFF images, with intensities ranging from 0 (white) to 255 (black).

2.7. CT scan image analysis

The reconstructed TIFF images were imported into MATLAB for image filtering. Since MICP and silica sand have similar densities (ρ_{MICP} =2.71 g/cm³ and ρ_{sand} =2.65 g/cm³), the pixel intensities of the two materials were very similar. To increase the contrast of the two materials, the range of intensities within the image slices were remapped to a larger range of intensities. For example, the original raw image had intensity values ranging from 66 to 89 for the MICP and sand. After adjusting the intensity of the image, the intensity range of the MICP and sand in the raw image was remapped from [66 89] to [25 255].

After improving the contrast between the MICP and test material, image filtering was used to decrease the noise in the image while still preserving the MICP phase. A 2-D median filter was applied to the image slices to reduce the salt and pepper noise predominately located within the sand grains. The filtered TIFF images were then imported into Dragonfly Pro (ORS, Canada) software for image thresholding, particle segmentation, and further analyses. Image thresholding was used to identify the range of pixel intensities that represents the sand grain, calcium carbonate precipitation, and pore space in the images. Quantifying the sand, calcium carbonate, and pore space pixels for each image slice allowed for an x-ray CT determined void ratio and calcium carbonate content to be calculated. Additional measurement tools in Dragonfly, such as watershed transformation and slice analysis, were used to label individual sand grains and study MICP trends.

There was likely some transition of MICP pixels to sand pixels during the filtering process due to the influence of neighboring pixels' intensity on the output pixel's intensity. To quantify the influence of image filtering on the x-ray CT determined calcium carbonate content, the image filtering process was performed in duplicate. Along the height of the CT specimen, there was less than 0.5% variation in calcium carbonate content between the two filtered image stacks.

3. Results

3.1. Evolution of soil stiffness

The two sands exhibited different improvements in soil stiffness during MICP treatment (Fig. 2). The soil with a smaller C_u exhibited a greater increase in V_s for the first 50 hours of MICP treatment. However, after 18 MICP-injections (approximately 160 hours), the sand with a larger C_u had approximately 100 m/s greater V_s. Similarly, after 30 MICP-injections, the final V_s of the sand with a larger C_u is greater than the sand with a C_u of 1.3. However, considering the limitations of the bender element system, such as a more difficult determination of the arrival time towards the end of MICP treatment (i.e., stiff soil with a harsh pore fluid environment), it is likely that the final V_s of the two sands is not significantly different. For a majority of the MICP treatment duration, the soil with a smaller C_u exhibited a greater V_s; however, the slope of the V_s increase with time is greater for the sand with a C_u of 3.8. These process monitoring observations indicate that sands with more particle contacts due to an increase in Cu have a delayed increase in stiffness as a result of MICP treatment.

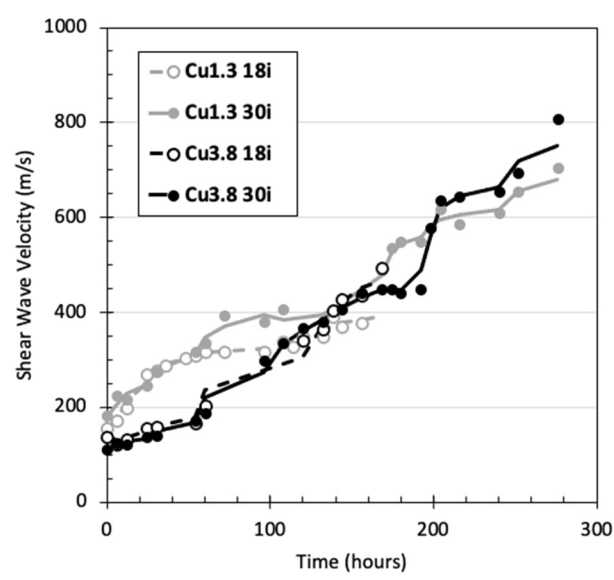


Figure 2. V_s of column specimen during MICP treatment. The trendline represents the three-point moving average. Note: 18i or 30i implies the specimen received either 18 or 30 MICP cementation injections, respectively.

3.2 Compressive strength

The UCS response of the column specimen are shown in Fig. 3. The UCS testing conditions, e.g. no confining or pore pressure, indicate the compressive strength is a result of MICP at particle-particle contacts. After receiving 18 MICP injections, the sand with a smaller C_u has a maximum unconfined compressive strength (q_u)

three times greater than that of the sand with a larger C_u for similar calcium carbonate contents (Fig. 4). All specimens were sheared at the same strain rate; however, the q_u of the C_u =1.3 sand occurs at a greater axial strain than the C_u =3.8 sand. Additionally, the reduction in stress after reaching q_u is greater for the sand with a smaller C_u , indicating a more brittle response. These results indicate that MICP-treated sand with a smaller C_u have a greater compressive strength for a moderate level of cementation (i.e., moderate levels of cementation as defined by Nafisi et al. 2020, Montoya and DeJong 2015).

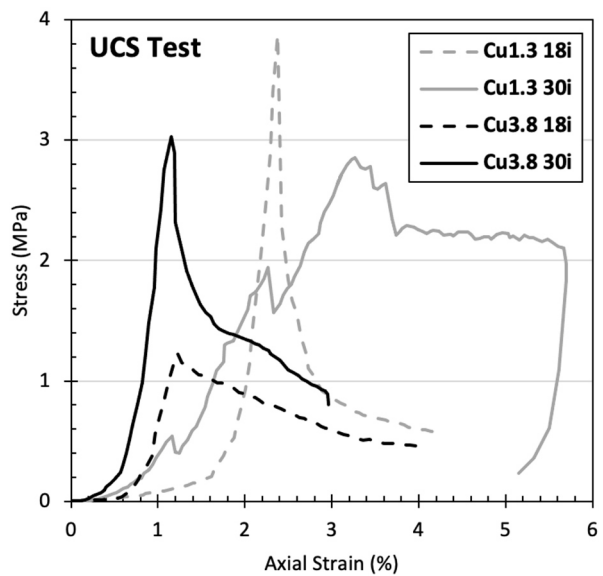


Figure 3. Stress-strain curves from UCS tests. Note: Cu1.3_30i exhibited localization prior to testing, therefore qu is not representative of the true capacity.

Increasing the number of MICP treatments from 18 to 30 for the C_u =3.8 sand resulted in an increase in V_s of 300 m/s; this in turn resulted in a 1.8 MPa increase in q_u . Both C_u =3.8 specimens experience q_u at approximately the same axial strain; however, the reduction in stress immediately following q_u is greater for the specimen with 30 MICP-injections. This observation indicates an increase in calcium carbonate content for the C_u =3.8 sand has a more brittle response.

A pre-existing localization was observed on the 30 MICP-injection C_u =1.3 sand specimen before running the UCS test. Therefore the increase in q_u from 18 to 30 MICP treatments for the C_u =1.3 sand cannot be assessed.

The localization in this specimen likely occurred during the extrusion process. During the UCS test, the pre-existing horizontal crack was observed to be the primary failure plane. Additional evidence of the localization is shown in Fig. 3, the specimen experienced two local q_u before reaching the global q_u . The reduction in compressive stress following the local peaks is likely a result of MICP bond breakage within the primary failure plane. Additional evidence of the localization is shown in Fig. 3, the specimen experienced two local q_u before reaching the global q_u .

The reduction in compressive stress following the local peaks is likely a result of MICP bond breakage within the primary failure plane.

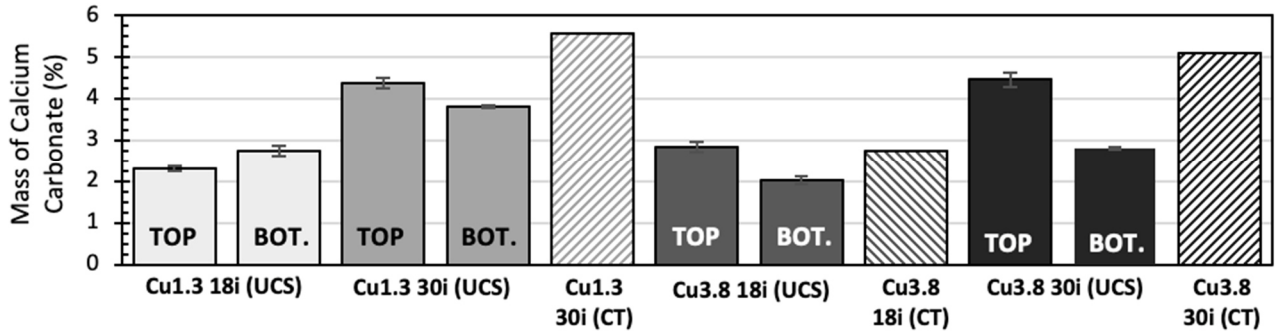


Figure 4. Calcium carbonate content of the UCS and CT specimen determined using gasometric acid washing techniques. The error bars represent one standard deviation.

However, after experiencing a reduction in stress, the load bearing chain within the specimen rearranged, allowing additional load to be supported. Despite the localization within the specimen, the q_u is not insignificant compared to the C_u=3.8 sands.

As previously mentioned, the current study administered the same number of MICP-injections to the two sand mixtures to study the influence of Cu on the level of improvement obtained after MICP treatment. The mass of calcium carbonate (%) for the UCS specimen with 18 MICP-injections was comparable, between 2 and 3% (Fig. 4). The Cu3.8 18i soil experienced a larger calcite content at the top of the specimen, compared to the Cu1.3 18i soil, which had the opposite trend. Because surface percolation methods were used and considering the pore size of the C_u=3.8 soil, the formation of MICP near the injection location may have resulted in partial closure of the pore network. The lower variability of calcite content within the MICPtreated C_u=1.3 soil suggests that the pore network was less affected. The mass of calcium carbonate for the UCS specimen with 30 MICP-injections both experienced greater cementation at the top of the specimen, with the C₁₁=3.8 soil having more MICP variability along the specimen height.

3.3 Microstructure observations

One goal of the current study is to draw a parallel between the MICP-treated CT and UCS specimen. According to Fig. 4, the calcium carbonate content of the CT specimen with a Cu of 3.8 and 18 MICP-injections falls within the range of the calcium carbonate content for the complimentary UCS specimen. However, the 30 MICP-treated CT specimen contains more MICP than the maximum MICP content of their respective UCS specimen, for both sands (Fig. 4). The authors have assumed the difference in calcium carbonate at this level of cementation has a negligible effect on MICP distribution within the soil fabric. Meaning, it is likely that the locations of MICP deposits and bonds between particles have been formed and any additional carbonate content would increase the deposit/bond size.

Vertical and horizontal slices from the x-ray CT scans are shown in Figs. 5 through 7. Image thresholding was applied to estimate the calcium carbonate content from the CT images. The Cu3.8_18i specimen was estimated to contain 1.2% mass of calcite from CT image thresholding, compared to the 2.8% that was measured in

the laboratory following the CT scan (Fig. 4). The lower calcium carbonate content measured from the CT image thresholding could be a result of several factors. An adverse effect of image filtering is smoothing pixel intensities at the interface of different materials, incorrectly labelling the calcite voxels on the soil particle's surface as sand instead of calcite. Another possibility could be that the mass of calcium carbonate unaccounted for has a particle size lower than the image resolution (1.18 μ m).

The specimen that received 30 MICP-injections had image thresholding MICP contents closer to the experimentally determined values shown in Fig. 4. Cu3.8_30i had a global calcium carbonate content of 5.8% determined from the CT data compared to 5.1%. Similarly, Cu1.3_30i had a global calcium carbonate content of 5.9% determined from the CT data and 5.6% determined in the laboratory.

Observations of the entire soil fabric, not limited to the two-dimensional slices, indicate the Cu3.8 18i specimen has significantly less MICP deposits compared to the Cu3.8 30i specimen. However, the experimentally determined (Fig. 4) calcium carbonate content of the Cu3.8 18i specimen is less than half that of the Cu3.8 30i specimen. The Cu3.8 30i specimen was observed to have discrete MICP deposits scattered across most particles surfaces, regardless of the host particle size. Whereas observations from the Cu3.8 18i indicate more random precipitation trends. The discrete deposits within the Cu3.8 30i specimen ranged between 10 and 30 µm in diameter. The Cu3.8 18i specimen contained less frequent discrete deposits. The occasional, large MICP deposits, up to 100 µm in diameter, were attached to both small and large sand grains within Cu3.8 30i.

Similar to the Cu3.8_30i specimen, the Cu1.3_30i specimen was observed to have small MICP deposits of similar size circumscribing the sand grains. However, the Cu1.3_30i specimen was observed to have more uniformity of these discrete deposits on all soil grains. The Cu3.8_30i specimen appeared to have more randomized MICP distribution within the sand matrix. At particle-particle contacts within the Cu1.3_30i soil, the discrete deposits on soil particle surfaces transitioned into continuous deposits at the contact points of similar thicknesses.

To better identify MICP uniformity along the length of the CT specimen, the local mass of calcium carbonate was evaluated for each XY slice and is shown in Fig. 8. Additionally, the image slice corresponding to the minimum and maximum local precipitation content for the 30 MICP-treated CT specimen are displayed. The standard deviation of the local MICP content for Cu1.3_30i, Cu3.8_18i, and Cu3.8_30i specimen are 1.84, 0.81, and 2.18, respectively.

The major difference in MICP trends observed in Images A and B is the presence of a large MICP bond, greater than 0.5 mm in length, in Image B.

Both Images A and B contain larger discrete MICP deposits than those observed in the C_u =1.3 soil. The local relative density of image A is 114% compared to -93%

in image B. The spike in local MICP content is likely due to the combined effect of the large MICP bond and the local relative density.

The MICP trends shown in Images C and D appear to be the same. Small, discrete precipitation is distributed across the surface area of all sand grains, regardless of MICP content. The local relative density of image C is 106% compared to -29% in image D. It is likely that the large difference in local MICP content, 3.54% (Image C) compared to 16.7% (Image D), is due to the larger void ratio in image D.

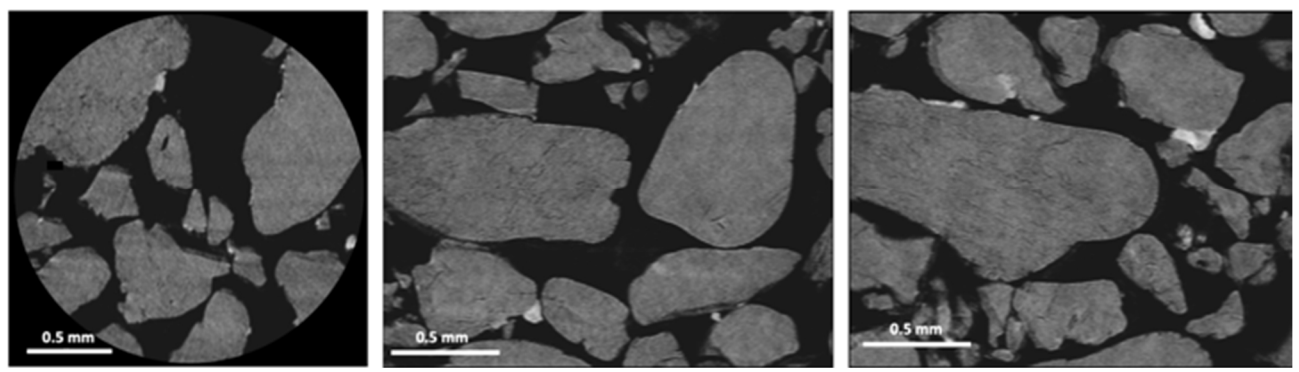


Figure 5. Horizontal (a) and vertical (b and c) image slices for the Cu=3.8 sand after 18 MICP injections (Cu3.8_18i_CT)

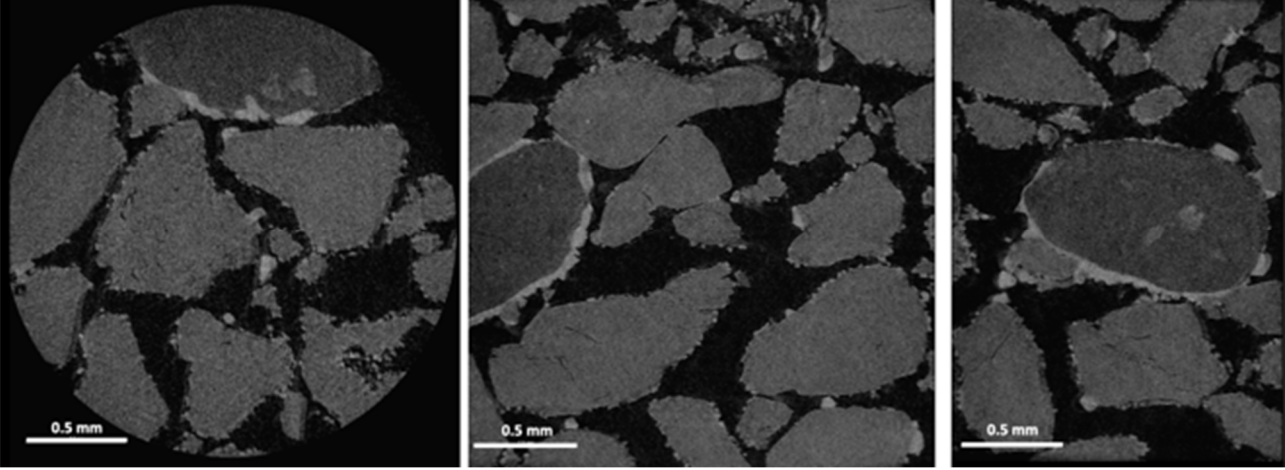


Figure 6. Horizontal (a) and vertical (b and c) image slices for the C_u=3.8 sand after 30 MICP injections (Cu3.8_30i_CT).

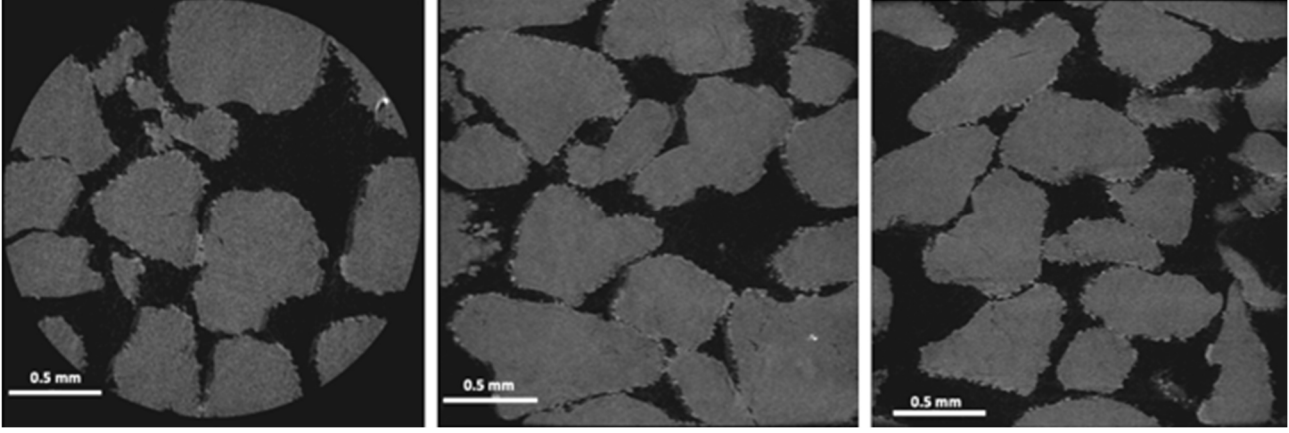


Figure 7. Horizontal (a) and vertical (b and c) image slices for the Cu=1.3 sand after 30 MICP injections (Cu1.3_30i_CT).

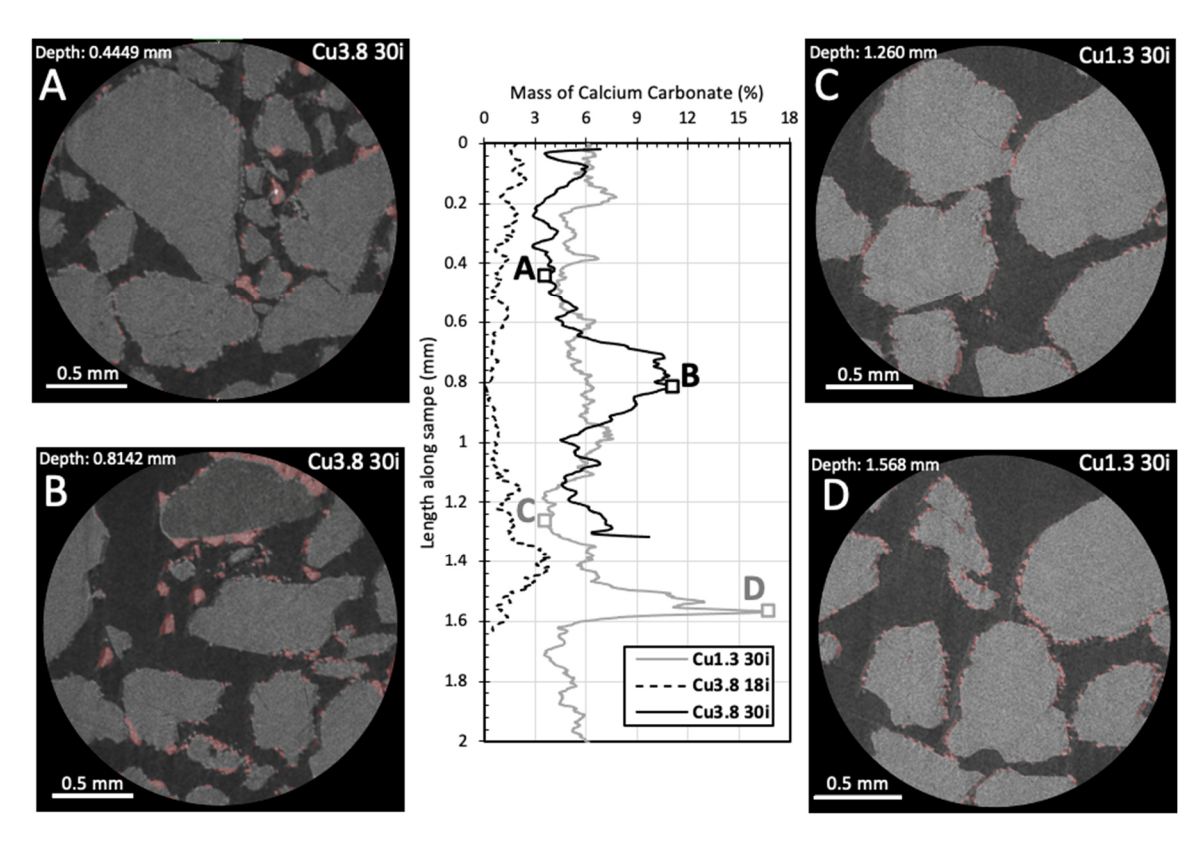


Figure 8. Local mass of calcium carbonate along CT specimen. The red shaded areas in Images A through D are defined as MICP from image thresholding techniques. Sub-figures A and B are from specimen Cu3.8_30i, and C and D are from specimen Cu1.3_30i; the locations of the horizontal slices are indicated along the specimen length plot in the center of the figure.

4. Discussion

In this study, the microstructure of MICP-treated sands with varying C_u was compared to the macroscale response. The evolution of soil stiffness was monitored during MICP treatment and UCS testing was performed at two levels of calcium carbonate content. X-ray CT imagery was performed on two specimens with a larger C_u at a moderate and heavy level of MICP and one specimen with a smaller C_u at a heavy level of cementation. This study is the first of its kind to examine sands with varying C_u using x-ray CT imaging techniques to better understand the effect of intrinsic sand characteristics on MICP efficiency.

Results from V_s monitoring indicates that the soil with a smaller C_u exhibited a greater increase in soil stiffness during the first 50 hours of MICP treatment, this is shown by the slope of the trendline in Fig. 2. However, after a calcium carbonate content threshold, the two sands show similar additional increase in V_s with time. These process monitoring observations indicate that sands with more particle contacts due to an increase in C_u have a delayed increase in stiffness as a result of MICP treatment.

These findings are consistent with a similar study on particle diameter and morphology (Nafisi et al. 2020). Nafisi et al. (2020) found that Ottawa 50-70 sand experienced a lag in V_s improvement during MICP treatment compared to Ottawa 20-30 sand. Nafisi et al. (2020) attributed the delayed increase in Vs to the increased number of particle contacts per volume associated with a smaller mean grain size. Additionally, the varying granular characteristics (D_{50} and particle

morphology) resulted in different calcium carbonate contents associated with similar levels of improvement (Nafisi et al. 2020).

Differences in particle size, morphology, and C_u are known to change the number and sizes of particle contacts within a soil matrix, ultimately influencing MICP efficiency. In this study, the sand mixture with a larger C_u has more particle contacts in the soil system due to the presence of varying particle sizes, making the observed V_s improvements shown in Fig. 2 to be consistent with conclusions from Nafisi et al. (2020). Future research that quantifies the contribution of individual intrinsic sand characteristics on the number and size of particle contacts may further elucidate the influence of soil fabric on the level of improvement that can be obtained from MICP.

Second, the improvement in soil stiffness resulting from MICP treatment does not equate to the same level of improvement in qu for different test materials. The Cu1.3_18i specimen had a Vs less than the Cu3.8_18i specimen for a similar MICP content; however, the qu was three times greater than the Cu3.8_18i specimen. Similarly, the Cu1.3_30i specimen had a lower Vs than the Cu3.8_30i and experienced localization prior to UCS testing, yet the qu were similar. If the Cu1.3_30i specimen had been undisturbed, it is likely that the qu would have been greater than that of the Cu3.8_30i soil.

Lastly, the randomized MICP distribution within the C_u =3.8 soil observed from x-ray CT suggest the macroscale response could be highly variable, especially at lower levels of MICP. For example, the large jump in V_s for Cu3.8_30i at approximately 200 hours could be a result of a particle-particle MICP bond altering the shear

wave propagation path through the medium. Additionally, the variability of large MICP bonds along the height of the C_u =3.8 specimen would influence the q_u . Future research should address the statistical variability of the level of improvement (e.g. q_u , friction angle, etc.) of MICP-treated soils with varying C_u .

Despite this study's contributions, some additional limitations should be addressed. First, it was assumed the MICP distribution within the CT and UCS specimen are similar; however, due to the differences in specimen size there could be slight differences. Future research may use SEM images of the UCS specimen to confirm the CT image observations on MICP distribution trends. Second, the localizations in the Cu1.3_30i specimen prevented the comparison of the Cu on qu level of improvement at a higher level of cementation. Future research may investigate if the same trends exist at light and heavy levels of cementation.

5. Conclusions

The results from V_s monitoring, UCS testing, and microstructure observations presented in this study have helped elucidate the influence of C_u on MICP formation and level of improvement achievable post-MICP treatment. Specifically:

- V_s monitoring indicates that sands with more particle contacts due to an increase in C_u have a delayed increase in stiffness as a result of MICP treatment.
- Maximum unconfined compressive strength of MICP-treated sands are dependent on both calcium carbonate content and C_u.
- X-ray CT images indicate more uniform MICP distribution within the soil fabric for sands with uniform particle size.

Additionally, this study provided insights into the applicability of x-ray CT scanning MICP-treated sands. Considering the availability and cost of conducting a CT scan, it may not be advantageous to perform scanning on MICP-treated sands with less than 3% calcium carbonate content. At low MICP contents, a higher pixel resolution is required to detect small MICP deposits; however, this will result in a smaller field of view that may not satisfy the representative elementary volume of the granular material. At higher calcium carbonate contents, CT scanning can detect MICP deposits on the surface of soil particles and at particle-particle contacts. However, to ensure x-ray CT scans provide a meaningful evaluation of soil microstructure, precaution should be used when calcium carbonate contents become much larger than what may be achievable in field applications.

Acknowledgements

This material is based upon work supported by the National Science Foundation Graduate Research Fellowship under Grant No. (DGE-2137100), and Grant Numbers CMMI-1933350 and 1934844. Any opinion, findings, and conclusions or recommendations expressed in this material are those of the authors and do not

necessarily reflect the views of the National Science Foundation. This work was performed in part at the Analytical Instrumentation Facility (AIF) at North Carolina State University, which is supported by the State of North Carolina and the National Science Foundation (ECCS #1542015). The AIF is a member of the North Carolina Research Triangle Nanotechnology Network (RTNN), a site in the National Nanotechnology Coordinated Infrastructure (NNCI).

References

- Baek, S.-H., Kwon, T.-H., and DeJong, J.T. "Impact of microbially induced calcite precipitation (MICP) on hydraulic conductivity of coarse sands", In: 20th International Conference on Soil Mechanics and Geotechnical Engineering, Sydney, Australia, 2022, pp. 4905-4909.
- Dadda, A., Geindreau, C., Emeriault, F., Du Roscoat, S.R., Garandet, A., Sapin, L. and Filet, A.E. "Characterization of microstructural and physical properties changes in biocemented sand using 3D X-ray microtomography", Acta Geotech, 12(5), pp.955-970, 2017. http://doi.org/10.1007/s11440-017-0578-5
- DeJong, J.T., Mortensen, B.M., Martinez, B.C. and Nelson, D.C. "Bio-mediated soil improvement", Ecol Eng, 36(2), pp.197-210, 2010. https://doi.org/10.1016/j.ecoleng.2008.12.029
- DeJong, J.T., Gomez, M.G., San Pablo, A.C.M., Graddy, C.M.R., Nelson, D.C., Lee, M., Ziotopoulou, K., El Kortbawi, M., Montoya, B., and Kwon, T.-H. "State of the Art: MICP soil improvement and its application to liquefaction hazard mitigation", In: 20th International Conference on Soil Mechanics and Geotechnical Engineering, Sydney, Australia, 2022, pp. 405-508.
- Lin, H., Suleiman, M.T., Brown, D.G. and Kavazanjian Jr, E. "Mechanical behavior of sands treated by microbially induced carbonate precipitation", J Geotech Geoenviron Eng, 142(2), 2016. http://doi.org/10.1061/(ASCE)GT.1943-5606.0001383
- Montoya, B.M., Gerhard, R., DeJong, J.T., Wilson, D.W., Weil, M.H., Martinez, B.C. and Pederson, L. "Fabrication, operation, and health monitoring of bender elements for aggressive environments", Geotech Test J, 35(5), pp. 728-742, 2012. https://doi.org/10.1520/GTJ103300
- Montoya, B.M. and DeJong, J.T. "Stress-strain behavior of sands cemented by microbially induced calcite precipitation", J Geotech Geoenviron Eng, 141(6), 2015. https://doi.org/10.1061/(ASCE)GT.1943-5606.0001302
- Nafisi, A., Montoya, B. M. and Evans, T. M. "Shear strength envelopes of biocemented sands with varying particle size and cementation level", J Geotech Geoenviron Eng, 146(3), 2020. https://doi.org/10.1061/(ASCE)GT.1943-5606.0002201
- O'Toole, C., Liu, Q., Montoya, B.M., Kananizadeh, N. and Odle, W. "The Effect of Microbial Induced Carbonate Precipitation on Fine-Grained Mine Tailings", In: Geo-Congress, Charlotte, USA, 2022, pp. 335-346. http://doi.org/10.1061/9780784484012.035
- Al Qabany, A. and Soga, K. "Effect of chemical treatment used in MICP on engineering properties of cemented soils." In: Bio-and Chemo-Mechanical Processes in Geotechnical Engineering: Géotechnique Symposium in Print, 2013, pp. 107-115. https://doi.org/10.1680/geot.SIP13.P.022
- Tagliaferri, F., Waller, J., Andò, E., Hall, S.A., Viggiani, G., Bésuelle, P. and DeJong, J.T. "Observing strain localisation processes in bio-cemented sand using x-ray imaging", Granul Matter, 13(3), pp. 247-250, 2011. https://doi.org/10.1007/s10035-011-0257-4